# Vibrational Spectra and Structure of $CH_3Cl:H_2O$, $CH_3Cl:HDO$, and $CH_3Cl:D_2O$ Complexes. IR Matrix Isolation and ab initio Calculations

**Nadia Dozova, Lahouari Krim,* M. Esmaïl Alikhani, and Nelly Lacome**

*LADIR/CNRS UMR 7075, Université Pierre et Marie Curie, Bat F74, case 49, 4 place Jussieu, 75252 Paris, Cedex 05, France*

*Received: July 15, 2005; In Final Form: September 15, 2005*

The infrared spectra of $CH_3Cl + H_2O$ isolated in solid neon at low temperatures have been investigated. The $CH_3Cl + H_2O$ system is remarkable because of its propensity to form $CH_3Cl:H_2O$ and $CH_3Cl:(H_2O)_n$ ($n \geq 2$) complexes. We focus here on the $CH_3Cl:H_2O$ species. Low concentration studies (0.01−0.5%) and subsequent annealing lead to formation of the 1:1 $CH_3Cl:H_2O$ complex with O−H···Cl−C or O···H−C intermolecular hydrogen bonds. Vibrational modes of this complex have been detected. In addition, spectra of $D_2O + CH_3Cl$ and $HDO + CH_3Cl$ have also been recorded. A detailed vibrational analysis of partially deuterated species shows that HDO is exclusively D bonded to $CH_3Cl$. This is a consequence of the preference for HDO to form a deuterium bonding complex rather than a hydrogen bonding one.

## Introduction

The water vapor content of the stratosphere varies[1] and thus determines the balance of chemical reactions in the stratosphere. This implies that the future chemical composition of the stratosphere is dependent on any interaction (weak or strong) between water and the reagents present. Studies on bound molecular complexes[2−4] where $H_2O$ interacts with other molecules of the stratosphere can improve our understanding of stratospheric reactions. Ideally, in the laboratory, such reactions should be carried out in the gas phase to make sure that the complex partners are moving free of any external perturbation. Such experiments, although they can be performed, are difficult to achieve, while the matrix isolation technique is an easier, more powerful tool for studying molecular complexes.

In the present study, the structure of the $CH_3Cl:H_2O$ complex was investigated by neon matrix isolation combined with infrared absorption spectroscopy. Detailed vibrational assignments were made from the observed spectra of the $CH_3Cl:H_2O$ complex. Using ab initio calculations, geometrical and vibrational properties of the complex have been estimated. In addition, spectra of $D_2O + CH_3Cl$ and $HDO + CH_3Cl$ samples have also been recorded and the vibrational wavenumbers for the four isotopic complexes $CH_3Cl:H_2O$, $CH_3Cl:DOH$, $CH_3Cl:HOD$, and $CH_3Cl:D_2O$ were calculated and compared with the observed values. All the wavenumbers of the observed bands on the partially deuterated complex are consistent with the calculated values of $CH_3Cl:DOH$, which proves the existence of the $CH_3Cl:DOH$ complex (HDO is D bonded to $CH_3Cl$), rather than $CH_3Cl:HOD$.

## Experimental Technique

$CH_3Cl + H_2O$ samples were prepared by co-condensing $CH_3Cl/H_2O/Ne$ mixtures onto a cryogenic metal mirror maintained at 5 K. Molar ratios (X/Ne, X = $CH_3Cl$ or $H_2O$) ranged from 0.001 to 1%. The experimental method and setup have been previously described in detail.[5] We shall recall only the main points. The deposition times were around 60 min. Neon and $CH_3Cl$ gases were obtained from "L'Air liquide" with purities of 99.9995 and 99.8%, respectively. $CH_3Cl$ was purified by using trap-to-trap vacuum distillations. D-Isotopic water (Euriso-top 99.90%) as well as natural water was degassed in a vacuum line. The purity of the samples was confirmed spectroscopically.

Infrared spectra of the resulting samples were recorded in the transmission-reflection mode between 4500 and 500 $cm^{-1}$ using a Bruker 120 Fourier transform infrared (FTIR) spectrometer equipped with a KBr/Ge beam splitter and a liquid-$N_2$-cooled narrow band HgCdTe photoconductor. A resolution of 0.1 $cm^{-1}$ was used. Bare mirror backgrounds, recorded from 4500 to 500 $cm^{-1}$ prior to sample deposition, were used as references in processing the sample spectra. Absorption spectra in the mid-infrared were collected on samples through a KBr window mounted on a rotatable flange separating the interferometer vacuum ($10^{-3}$ mbar) from that of the cryostatic cell ($10^{-7}$ mbar). The spectra were subsequently subjected to baseline correction to compensate for infrared light scattering and interference patterns. All spectra were recorded at 5 K.

The samples could be irradiated using a 200 W mercury−xenon high pressure arc lamp and either interference narrow (5 nm full width at half-maximum (fwhm)) or broad band filters in order to find if some photoprocesses could be initiated by UV−visible or near-infrared light. Next, or after sample annealing up to 12 K in several steps, infrared spectra of the samples were recorded again between 4500 and 500 $cm^{-1}$ as outlined above.

## Experimental Results

**$CH_3Cl$ in Ne Matrix.** Spectra of pure $CH_3Cl$ isolated in neon matrixes have been recorded at 5 K at different concentrations of $CH_3Cl$ and have been previously described.[6] Briefly, the C−Cl stretching region (Figure 1a) has two sets of bands belonging to the two isotopomers $CH_3{}^{35}Cl$ and $CH_3{}^{37}Cl$. Each band consists of three sharp peaks due to splitting by the matrix

* To whom correspondence should be addressed. E-mail: krim@ccr.jussieu.fr.

10.1021/jp053895g CCC: $30.25 
Published on Web 10/13/2005

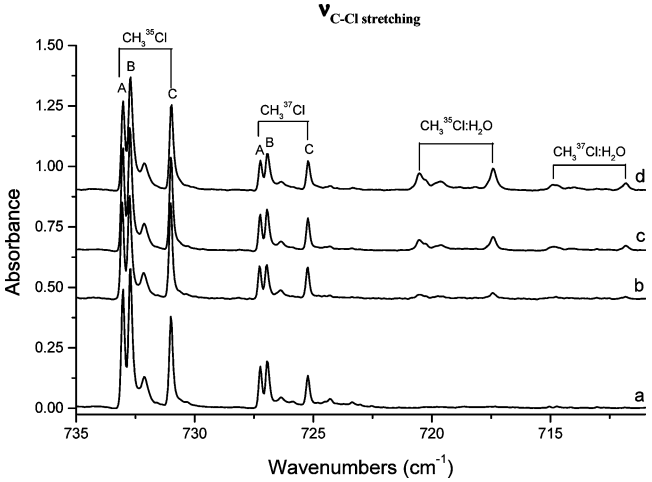


**Figure 1.** C−Cl stretching ($\upsilon_{3\ CH_3Cl}$) region of $CH_3Cl$ and the $CH_3Cl$:$H_2O$ complex after deposition at 5 K: (a) $CH_3Cl/Ne = 5{:}10\ 000$; (b) $CH_3Cl/H_2O/Ne = 5{:}2.5{:}10\ 000$; (c) $CH_3Cl/H_2O/Ne = 5{:}5{:}10\ 000$; (d) $CH_3Cl/H_2O/Ne = 5{:}10{:}10\ 000$.

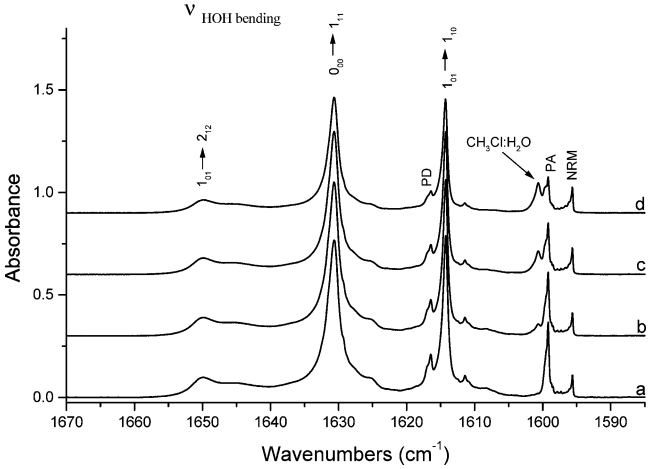


**Figure 2.** HOH bending ($\upsilon_2$) region of $H_2O$ and the $CH_3Cl$:$H_2O$ complex after deposition at 5 K: (a) $H_2O/Ne = 5{:}10\ 000$; (b) $CH_3Cl/H_2O/Ne = 1.5{:}5{:}10\ 000$; (c) $CH_3Cl/H_2O/Ne = 5{:}5{:}10\ 000$; (d) $CH_3Cl/H_2O/Ne = 10{:}5{:}10\ 000$.

cage. For the $CH_3{}^{35}Cl$ isotopomer, they are situated at 733.0 $cm^{-1}$ (peak A), 732.7 $cm^{-1}$ (peak B with a shoulder at 732.1 $cm^{-1}$), and 731.0 $cm^{-1}$ (peak C), while, for the other isotopomer, they are located at 727.2 $cm^{-1}$, 726.9 $cm^{-1}$ (with a shoulder at 726.3 $cm^{-1}$), and 725.2 $cm^{-1}$, respectively. The shift between two corresponding peaks in the two isotopomers is 5.8 $cm^{-1}$. Upon annealing (11−12 K), only the band of site B remains intense, which characterizes the most stable site of $CH_3Cl$ trapped in the neon matrix.

In the region of C−H symmetric stretching (and also for other vibrational modes of $CH_3Cl$), three peaks are observed; each of them is correlated with one of peaks A, B, and C in the C−Cl stretching mode region. Vibrational mode frequencies of $CH_3Cl$ trapped in the most stable site in the neon matrix (site B) are given in Table 1. In the following, we will take the C−Cl stretching spectral region as a characteristic domain of the specific vibrational modes of the $CH_3Cl$ monomer and $CH_3Cl$:$H_2O$ complex.

**$H_2O$ in Ne Matrix.** Rovibrational spectra of water monomers trapped in solids have been the subject of several studies.[7−11] $H_2O$ rovibrational transitions are labeled $J''_{K''_aK''_c} \rightarrow J'_{K'_aK'_c}$, where $J$ is the quantum number associated with the total rotational angular momentum and $K_a$ and $K_c$ are the quantum numbers of the components of $J$ on the principal axes $a$ and $c$, respectively.[11−13] Due to the symmetry point group of water ($C_{2v}$), the hydrogen atoms are equivalent and may possess antiparallel ($p$-$H_2O$) or parallel ($o$-$H_2O$) nuclear spins. The ground state for the para and ortho molecules are the $0_{00}$ and $1_{01}$ levels, respectively. A nuclear spin conversion (NSC) process occurs between the $1_{01}$ rotational level (metastable level) and the $0_{00}$ ground level.[13]

Isolation in rare gas solids such as argon and neon shows that two kinds of water molecules are spectroscopically distinguishable: the rotating monomer (RM) which gives rise to several rovibrational lines starting from $J'' = 0$ or 1 and the nonrotating momomer (NRM) for which rotation is hindered either by the matrix inhomogeneity or by weak interactions between non-nearest neighbors and which gives rise to a transition close to the pure vibrational frequencies.[7−9] It should be noticed that water monomers trapped in molecular solids, such as $N_2$ and normal $-D_2$, do not rotate with the exception of solid $H_2$.[13] The three vibrational fundamentals are labeled $\nu_2$ (HOH bending), $\nu_1$ (symmetric stretching), and $\nu_3$ (antisymmetric stretching).

*$\nu_2$ Mode.* Figure 2a shows the infrared absorption spectrum of a $H_2O$/Ne sample deposited at 5 K in the $\nu_2$ region (HOH bending). The three most intense peaks of rotating $H_2O$ molecules are situated at 1614.2 $cm^{-1}$ (rovibrational transition $1_{01} \rightarrow 1_{10}$), 1630.6 $cm^{-1}$ ($0_{00} \rightarrow 1_{11}$), and 1649.9 $cm^{-1}$ ($1_{01} \rightarrow 2_{12}$). The NRM peak is located at 1595.6 $cm^{-1}$ (characterized by an intensity increase with concentration and by an intensity decrease upon annealing). The other two intense peaks belong to the $H_2O$ dimer: the one at 1599.2 $cm^{-1}$ belongs to the proton acceptor (PA) and the other at 1616.4 $cm^{-1}$ to the proton donor (PD).[14]

**TABLE 1: Vibrational Mode Frequencies (in $cm^{-1}$) of $CH_3Cl$ (Site B), $H_2O$ (Nonrotating Monomer (NRM)), and the $CH_3Cl$:$H_2O$ Complex in a Neon Matrix**

| mode | | monomer/Ne | $CH_3Cl$:$H_2O$/Ne | shift[a] |
|---|---|---|---|---|
| | | $CH_3Cl$ | | |
| C−Cl stretching | $\upsilon_{3\ CH_3Cl}$ | 726.9 ($^{37}Cl$) | 714.8 | −12.1 |
| | | 732.7 ($^{35}Cl$) | 720.5 | −12.2 |
| C−Cl rocking | $\upsilon_{6\ CH_3Cl}$ | 1019.4 | 1022.2 | 2.8 |
| C−H symmetric bending | $\upsilon_{2\ CH_3Cl}$ | 1354.8 | 1357.3 | 2.5 |
| C−H antisymmetric bending | $\upsilon_{5\ CH_3Cl}$ | 1451.5 | 1455.2 | 3.7 |
| C−H symmetric stretching | $\upsilon_{1\ CH_3Cl}$ | 2967.5 | 2972.2 | 4.7 |
| C−H antisymmetric stretching | $\upsilon_{4\ CH_3Cl}$ | 3036.7 | 3044.2 | 7.5 |
| | | $H_2O$ | | |
| O−H bending | $\upsilon_{2\ H_2O}$ | 1595.6 | 1600.5 | 4.9 |
| O−H symmetric stretching | $\upsilon_{1\ H_2O}$ | 3665.5 | 3625.9 | −39.6 |
| O−H antisymmetric stretching | $\upsilon_{3\ H_2O}$ | 3761.1 | 3738.8 | −22.3 |

[a] shift = $\upsilon_{complex} - \upsilon_{free\ molecule}$.

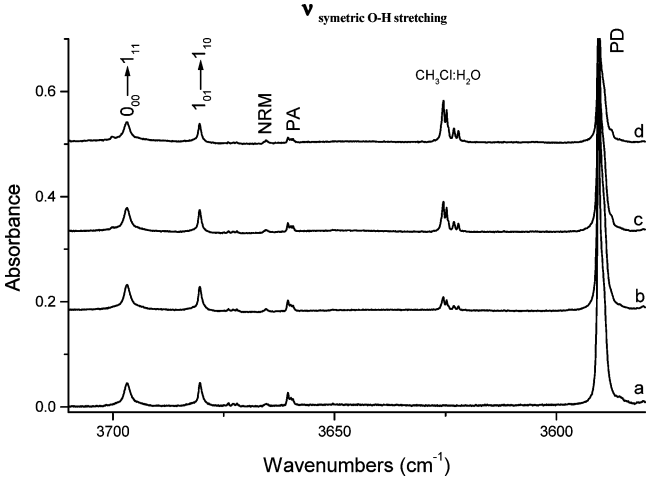


**Figure 3.** O−H symmetric stretching ($\upsilon_1$) region of $H_2O$ and the $CH_3Cl:H_2O$ complex after deposition at 5 K: (a) $H_2O$/Ne = 5:10 000; (b) $CH_3Cl/H_2O$/Ne = 1.5:5:10 000; (c) $CH_3Cl/H_2O$/Ne = 5:5:10 000; (d) $CH_3Cl/H_2O$/Ne = 10:5:10 000.

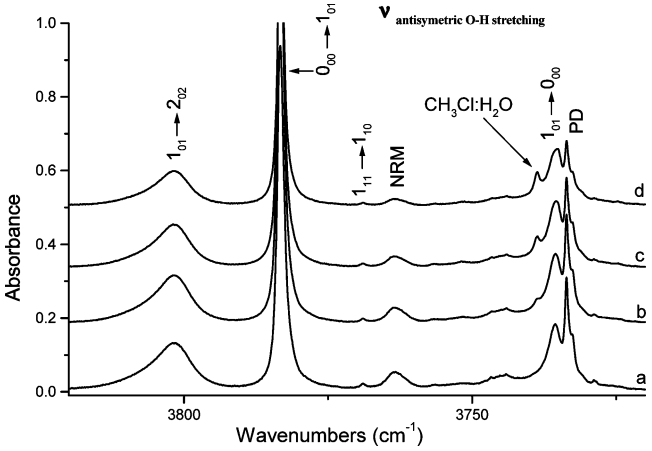


**Figure 4.** O−H antisymmetric stretching ($\upsilon_3$) region of $H_2O$ and the $CH_3Cl:H_2O$ complex after deposition at 5 K: (a) $H_2O$/Ne = 5:10 000; (b) $CH_3Cl/H_2O$/Ne = 1.5:5:10 000; (c) $CH_3Cl/H_2O$/Ne = 5:5:10 000; (d) $CH_3Cl/H_2O$/Ne = 10:5:10 000.

*$\nu_1$ Mode.* Figure 3a shows the symmetric O−H stretching region ($\nu_1$). Two bands of the rotating monomer are observed at 3680.4 cm$^{-1}$ ($1_{01} \rightarrow 1_{10}$) and 3696.9 cm$^{-1}$ ($0_{00} \rightarrow 1_{11}$). The PA band of the water dimer is situated at 3660.5 cm$^{-1}$ and the PD band (very intense) at 3590.5 cm$^{-1}$. The nonrotating monomer (NRM) band is detected at 3665.5 cm$^{-1}$. The NRM band (in solid neon) has been observed by Nelander et al.[9] and Forney et al.[10] at 3664.8 and 3660.6 cm$^{-1}$, respectively. Our observation is comparable with that reported by Nelander et al.[9] The band at 3660.6 reported by Forney et al.[10] could not be due to the water monomer but to $(H_2O)_2$. Indeed, the intensity of this band increases upon annealing. This result is confirmed by the recent work of Perchard et al.[14] who attributed this band to the $\nu_1$ mode of the $(H_2O)_2$ proton acceptor.

*$\nu_3$ Mode.* Figure 4a shows the antisymmetric O−H stretching region. The three most intense peaks of rotating $H_2O$ molecules are situated at 3735.7 ($1_{01} \rightarrow 0_{00}$), 3783.3 ($0_{00} \rightarrow 1_{01}$), and 3801.7 cm$^{-1}$ ($1_{01} \rightarrow 2_{02}$). The PA band of the water dimer situated at 3750.0 cm$^{-1}$ and the PD band at 3733.7 cm$^{-1}$ have been largely studied by Perchard et al.[14] The band of the nonrotating water monomer (NRM) is situated at 3761.1 cm$^{-1}$. The NRM band (in solid neon) has been observed by Nelander et al.[9] and Perchard et al.[14] at 3760.9 and 3760.8 cm$^{-1}$, respectively, which is comparable with our observation.

**TABLE 2: Frequencies (cm$^{-1}$) and Assignments of Absorption Lines of Monomeric $H_2O$**

| transition | gas phase[15] | solid argon[7,8] | solid neon (this work) | solid neon[10] |
|---|---|---|---|---|
| | | $\nu_2$ Region | | |
| NRM[a] | | 1589.2 | 1595.6 | 1595.6 |
| 101 → 110 ortho | 1616.714 | 1607.9 | 1614.2 | 1614.2 |
| 000 → 111 para | 1634.970 | 1623.8 | 1630.6 | 1630.6 |
| 101 → 212 ortho | 1653.268 | 1636.5 | 1649.9 | 1649.8 |
| | | $\nu_1$ Region | | |
| NRM[a] | | 3638.3 | 3665.5 | 3660.6 |
| 101 → 110 ortho | 3674.697 | 3653.5 | 3680.4 | 3680.6 |
| 000 → 111 para | 3693.294 | 3669.7 | 3696.9 | 3696.9 |
| | | $\nu_3$ Region | | |
| 101 → 000 ortho | 3732.135 | 3711.3 | 3735.7 | 3735.6 |
| NRM[a] | | 3736.0 | 3761.1 | |
| 000 → 101 para | 3779.493 | 3756.6 | 3783.3 | 3783.3 |
| 101 → 202 ortho | 3801.420 | 3776.4 | 3801.7 | 3801.7 |

[a] NRM: nonrotating molecule.

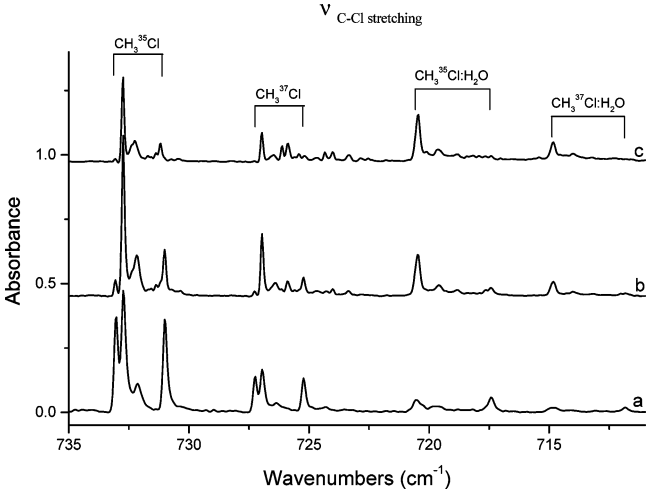


**Figure 5.** Annealing effects on $CH_3Cl:H_2O$ bands in the C−Cl stretching mode ($\upsilon_{3\ CH_3Cl}$) region for a sample with $CH_3Cl/H_2O$/Ne = 5:1:10 000: (a) after deposition at 5 K; (b) after annealing to 11 K; (c) after annealing to 12 K. All spectra are recorded at 5 K.

The transition frequencies attributed to the rotating and nonrotating $H_2O$ are given in Table 2 and compared to data in the literature.

**$CH_3Cl:H_2O$ in Ne Matrix.** When $CH_3Cl$ and $H_2O$ are co-deposited in a neon matrix, new bands appear in the vibrational regions of both $CH_3Cl$ and $H_2O$. Bands that grow linearly with the concentrations of both $CH_3Cl$ and $H_2O$ are assigned to the complex $CH_3Cl:H_2O$. Experiments are carried out at very low concentrations of $H_2O$ and $CH_3Cl$ in neon matrix to limit the aggregation processes. Under these conditions, $CH_3Cl:H_2O$ bands become predominant.

*C−Cl Region.* The evolution of these new bands as a function of $H_2O$ concentration in the region of the C−Cl stretching is shown in Figure 1, and their evolution upon annealing is shown in Figure 5. Absorption frequencies of the new bands are characterized by set I—720.5, 720.2 (shoulder), 719.6, and 717.4 cm$^{-1}$—and set II—714.8, 714.6 (shoulder), 714.0, and 711.8 cm$^{-1}$. The relative intensity of 3:1 between sets I and II indicates that set I belongs to the $CH_3{}^{35}Cl:H_2O$ isotopomer, while set II belongs to $CH_3{}^{37}Cl:H_2O$. The shift between the bands of the two isotopomers is 5.6 cm$^{-1}$. The four bands for each $CH_3Cl:H_2O$ isotopomer are probably due to the fact that different sites are occupied by the complex in the Ne matrix (similar to what is observed in the case of $CH_3Cl$ monomer). This is confirmed

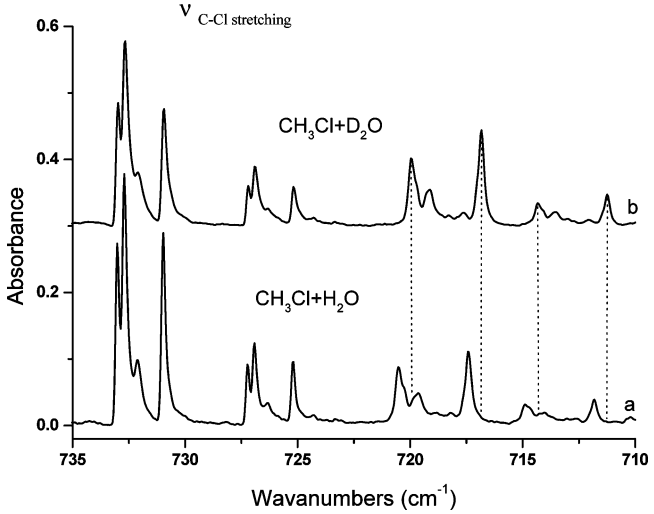


**Figure 6.** C−Cl stretching ($\upsilon_{3\ CH_3Cl}$) region of $CH_3Cl:H_2O$ and $CH_3Cl:D_2O$ after deposition at 5 K: (a) $CH_3Cl/H_2O/Ne$ = 5:5:10 000; (b) $CH_3Cl/D_2O/Ne$ = 5:5:10 000.

by the annealing effects shown in Figure 5. Upon annealing to 11 K, like in the case of $CH_3Cl$ monomer bands, only the two bands at 720.5 and 714.8 $cm^{-1}$ increase considerably (Figure 5b), showing that they correspond to the most stable site of the complex for the two isotopes ($CH_3{}^{35}Cl:H_2O$ and $CH_3{}^{37}Cl:H_2O$). Finally, $CH_3{}^{35}Cl:(H_2O)_2$ and $CH_3{}^{37}Cl:(H_2O)_2$ bands have also been observed at 706.9 and 701.4 $cm^{-1}$, respectively, but they will not be discussed in this paper ($CH_3Cl:(H_2O)_2$ has been left for future study). All vibrational mode frequencies of $CH_3Cl$ and $CH_3Cl:H_2O$ are listed in Table 1.

*$H_2O$ Region.* The evolution of the bands of the $CH_3Cl:H_2O$ complex with respect to the concentration of $CH_3Cl$ in the HOH bending ($\nu_2$), O−H symmetric stretching ($\nu_1$), and O−H antisymmetric stretching ($\nu_3$) regions is given in Figures 2, 3, and 4, respectively. The $\nu_2$, $\nu_1$, and $\nu_3$ bands of the complex are situated at 1600.5, 3625.9, and 3738.8 $cm^{-1}$, respectively. The symmetric stretching $\nu_1$ band consists of four peaks at 3625.9, 3624.8, 3623.1, and 3622.1 $cm^{-1}$. These peaks are probably due to site splitting and are related to the different peaks of $CH_3Cl:H_2O$ in the C−Cl stretching region. Upon annealing between 7 and 11 K, $CH_3Cl:H_2O$ bands increase. They remain constant or slightly decrease at 12 K. All $CH_3Cl:H_2O$ vibrational mode frequencies and shifts ($\nu_{complex} - \nu_{monomer}$) are summarized in Table 1.

Finally, the $CH_3Cl:H_2O$ complex has been irradiated by UV−visible or near-infrared light in order to initiate some photoprocesses, but no photochemical reactions were observed.

**$CH_3Cl:D_2O$ and $CH_3Cl:HDO$ in Ne Matrix.** *C−Cl Region.* Infrared spectra for different samples with $CH_3Cl/H_2O/Ne$ and $CH_3Cl/D_2O/Ne$ in the C−Cl stretching region are shown in Figure 6. As already reported, the bands for the most stable site of the $CH_3Cl:H_2O$ complex are situated at 720.5 $cm^{-1}$ ($CH_3{}^{35}Cl:H_2O$) and 714.8 $cm^{-1}$ ($CH_3{}^{37}Cl:H_2O$), as shown in Figure 6a. The bands of $CH_3Cl:D_2O$ have the same structure as the bands of $CH_3Cl:H_2O$ but are slightly red shifted (Figure 6b); thus, the bands of the most stable site of $CH_3Cl:D_2O$ are located at 719.9 $cm^{-1}$ ($CH_3{}^{35}Cl:D_2O$) and 714.3 $cm^{-1}$ ($CH_3{}^{37}Cl:D_2O$). In contrast with the C−Cl stretching mode, H/D isotopic substitutions in $H_2O$ monomer have no influence on the vibrational mode frequencies of the complex in the other spectral regions of $CH_3Cl$. In samples where HDO predominates, vibrational modes frequencies of $CH_3Cl:HDO$, in the area of $CH_3Cl$, are equal to those measured for $CH_3Cl:D_2O$.

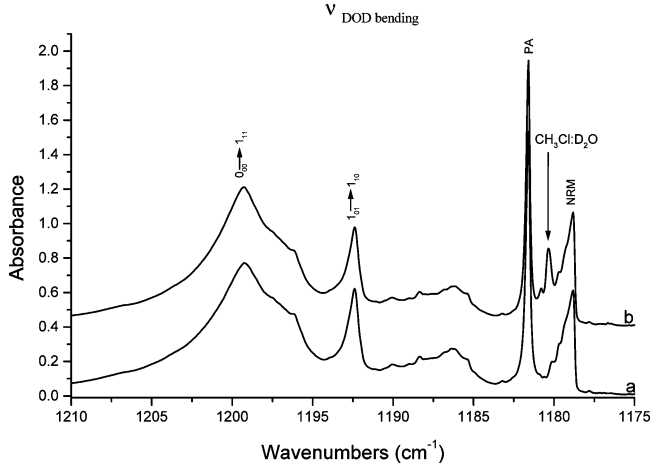


**Figure 7.** DOD bending ($\upsilon_2$) region of $D_2O$ and the $CH_3Cl:D_2O$ complex after deposition at 5 K: (a) $D_2O/Ne$ = 5:10 000; (b) $CH_3Cl/D_2O/Ne$ = 5:5:10 000.

**TABLE 3: Frequencies ($cm^{-1}$) and Assignments of Absorption Lines of Monomeric $D_2O$**

| transition | gas[16−18] | solid argon[10] | solid neon (this work) | solid neon[10] |
|---|---|---|---|---|
| | | $\nu_2$ Region | | |
| NRM[a] | | 1174.6 | 1178.8 | 1178.7 |
| 000 → 111 ortho | 1199.793 | 1196.0 | 1199.3 | 1199.3 |
| 101 → 212 para | 1209.388 | 1206.0 | 1206.7 | 1206.7 |
| | | $\nu_1$ Region | | |
| NRM[a] | | 2657.7 | 2676.7 | 2672.7 |
| 101 → 101 para | 2681.894 | 2667.8 | 2686.6 | 2686.6 |
| 000 → 111 ortho | 2691.606 | 2677.3 | 2695.4 | 2695.8 |
| | | $\nu_3$ Region | | |
| NRM[a] | | 2771.1 | 2785.9 | *b* |
| 000 → 101 ortho | 2799.759 | 2783.0 | 2801.6 | 2801.6 |
| 101 → 202 para | 2811.214 | 2795.0 | 2811.6 | 2811.3 |

[a] NRM: nonrotating molecule. [b] Not observed.

*$D_2O$ Region.* $D_2O$ spectral regions are similar to those of $H_2O$. However, they are spectrally more compact due to the smaller rotational constant of $D_2O$.[10] Figure 7a shows the $\nu_2$ $D_2O$ spectral region. The most intense peaks of rotating $D_2O$ molecules are situated at 1199.3 $cm^{-1}$ ($1_{01} \rightarrow 1_{10}$ states) and 1206.7 $cm^{-1}$ ($0_{00} \rightarrow 1_{11}$). The NRM peak is located at 1178.8 $cm^{-1}$. Another intense peak at 1181.2 $cm^{-1}$ belongs to the proton acceptor (PA) of $(D_2O)_2$.[10] A summary of $D_2O$ data and assignments is given in Table 3. When $CH_3Cl$ and $D_2O$ are co-deposited in a neon matrix, a new band due to the complex $CH_3Cl:D_2O$ appears at 1180.3 $cm^{-1}$ in the $\nu_2$ region (Figure 7). In the $\nu_1$ and $\nu_3$ mode regions, the NRM bands are located at 2676.7 and 2785.9 $cm^{-1}$, respectively, while bands belonging to the complex $CH_3Cl:D_2O$ are situated at 2649.8 and 2767.4 $cm^{-1}$, respectively. These results are summarized in Table 4.

*HDO Region.* HOD spectral regions are similar to those of $H_2O$ and $D_2O$. In the HDO molecule, the two O−D and O−H bonds are no longer equivalent. $\nu_1$ corresponds to the O−D stretching mode, and $\nu_3$ corresponds to the O−H stretching mode. The HOD bending mode ($\nu_2$) is situated at 1404.2 $cm^{-1}$, the O−D stretching mode ($\nu_1$), at 2727.4 $cm^{-1}$, and the O−H stretching mode ($\nu_3$), at 3706.6 $cm^{-1}$. Rovibrational transitions have also been assigned and compared to data from the literature (see Table 5). Spectra of the DOH bending region are shown in Figure 8. A band belonging to the complex $CH_3Cl:HDO$ is situated at 1399.7 $cm^{-1}$. Finally, the O−D and O−H stretching modes of $CH_3Cl:HDO$ are observed at 2681.5 and 3704.8 $cm^{-1}$, respectively. These results are summarized in Table 4.

**TABLE 4: Vibrational Mode Frequencies (in $cm^{-1}$) of the $CH_3Cl:H_2O$, $CH_3Cl:HDO$, and $CH_3Cl:D_2O$ Complexes in a Neon Matrix**

| mode | $CH_3Cl$ | water monomer | complex | shift |
|---|---|---|---|---|
| | | $H_2O$ | $CH_3Cl:H_2O$ | |
| $\upsilon_{3\ CH_3Cl}$ ($^{37}Cl$) | 726.9 | | 714.8 | −12.1 |
| $\upsilon_{3\ CH_3Cl}$ ($^{35}Cl$) | 732.7 | | 720.5 | −12.2 |
| $\upsilon_{2\ H_2O}$ | | 1595.6 | 1600.5 | 4.9 |
| $\upsilon_{1\ H_2O}$ | | 3665.5 | 3625.9 | −39.6 |
| $\upsilon_{3\ H_2O}$ | | 3761.1 | 3738.8 | −22.3 |
| | | HDO | $CH_3Cl:HDO$ | |
| $\upsilon_{3\ CH_3Cl}$ ($^{37}Cl$) | 726.9 | | 714.3 | −12.6 |
| $\upsilon_{3\ CH_3Cl}$ ($^{35}Cl$) | 732.7 | | 719.9 | −12.8 |
| $\upsilon_{2\ HDO}$ | | 1404.2 | 1399.7 | −4.5 |
| $\upsilon_{1\ HDO}$ | | 2727.4 | 2681.5 | −45.9 |
| $\upsilon_{3\ HDO}$ | | 3706.6 | 3704.8 | −1.8 |
| | | $D_2O$ | $CH_3Cl:D_2O$ | |
| $\upsilon_{3\ CH_3Cl}$ ($^{37}Cl$) | 726.9 | | 714.3 | −12.6 |
| $\upsilon_{3\ CH_3Cl}$ ($^{35}Cl$) | 732.7 | | 719.9 | −12.8 |
| $\upsilon_{2\ D_2O}$ | | 1178.8 | 1180.3 | 1.5 |
| $\upsilon_{1\ D_2O}$ | | 2676.7 | 2649.8 | −26.9 |
| $\upsilon_{3\ D_2O}$ | | 2785.9 | 2767.4 | −18.5 |

**TABLE 5: Frequencies ($cm^{-1}$) and Assignments of Absorption Lines of Monomeric HDO**

| transition | gas[15,19] | solid argon[10] | solid neon (this work) | solid neon[10] |
|---|---|---|---|---|
| | | $\nu_2$ Region | | |
| NRM[a] | | 1398.8 | 1404.2 | 1404.2 |
| 000 → 101 | 1419.041 | 1414.0 | 1419.1 | 1419.0 |
| 000 → 111 | 1435.300 | 1428.0 | 1433.5 | 1433.2 |
| | | $\nu_1$ Region | | |
| 101 → 000 | 2708.172 | | 2712.6 | 2712.7 |
| NRM[a] | | 2710.0 | 2727.4 | 2722.9 |
| 000 → 101 | 2738.914 | 2724.7 | 2742.2 | 2742.3 |
| | | $\nu_3$ Region | | |
| NRM[a] | | 3687.3 | 3706.6 | 3699.0 |
| 000 → 111 | 3736.160 | 3716.0 | 3728.7 | 3728.9 |
| 101 → 212 | 3748.720 | - | 3739.8 | 3739.3 |

[a] NRM: nonrotating molecule.

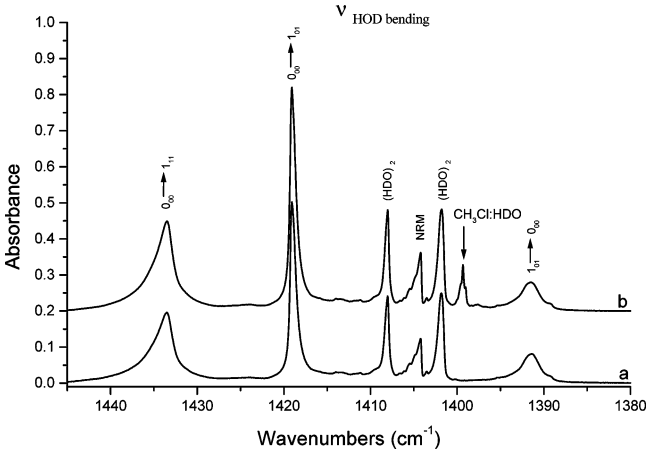


**Figure 8.** HOD bending ($\upsilon_2$) region of HDO and the $CH_3Cl:HDO$ complex after deposition at 5 K: (a) $H_2O$ + HDO/Ne = 5:10 000; (b) $CH_3Cl/H_2O$ + HDO/Ne = 5:5:10 000.

## Discussion

The wavenumber shifts of the $CH_3Cl:H_2O$ complex from $H_2O$ monomer are measured to be −39.6 and −22.3 $cm^{-1}$ for OH symmetric and antisymmetric stretching modes, respectively, and +4.9 $cm^{-1}$ for the HOH bending mode. The OH symmetric and antisymmetric stretching modes are red shifted, with respect to $H_2O$ monomer, by −1.1 and −0.6%, respectively, and the HOH bending mode is blue shifted by +0.31%. $D_2O$ and $D_2O:CH_3Cl$ spectral observations give the same trends for OD symmetric (−1%) and antisymmetric stretching ( −0.61%) modes, but the DOD bending mode is blue shifted by only +0.13% (less than half in comparison with the HOH bending shift). However, the partially deuterated $CH_3Cl:HDO$ complex exhibits red shifts from HDO monomer, for all HDO vibrational modes. The OD stretching, OH stretching, and HOD bending modes are red shifted by −1.7, −0.05, and −0.32%, respectively.

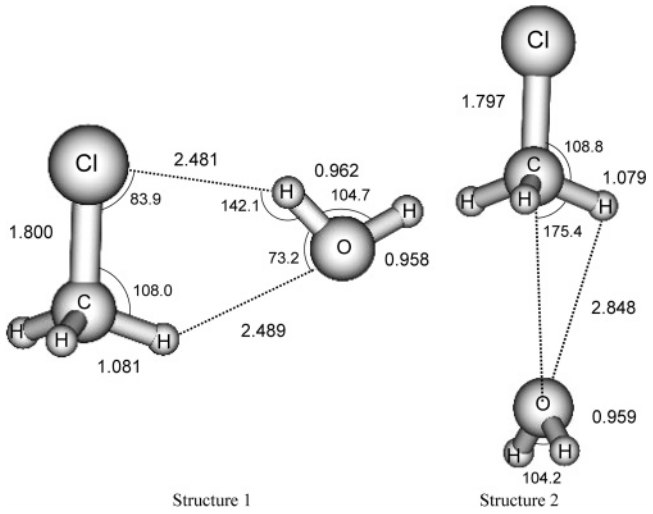


**Figure 9.** Calculated geometries of the two stable structures of the $CH_3Cl:H_2O$ complex.

From $CH_3Cl$ monomer, the complex exhibits blue shifts for all vibrational modes with the exception of the C−Cl stretching mode which is red shifted by −12.2 and −12.8 $cm^{-1}$ for $CH_3{}^{35}Cl:H_2O$ and $CH_3{}^{35}Cl:D_2O$, respectively. Since the bands of $CH_3Cl:D_2O$ and $CH_3Cl:HDO$ overlap with each other in all $CH_3Cl$ spectral regions, the wavenumber shifts of $CH_3Cl:D_2O$ and $CH_3Cl:HDO$, with respect to $CH_3Cl$ monomer, are the same.

The C−Cl rocking mode, the C−H symmetric bending mode, and the C−H antisymmetric bending mode are blue shifted by +2.8, +2.5, and +3.7 $cm^{-1}$, respectively. For the C−H symmetric and antisymmetric stretching modes, larger blue shifts are measured: +4.7 and +7.5 $cm^{-1}$, respectively. The wavenumber shifts for all of these vibrational modes are not sensitive to the $H_2O/D_2O$ isotopic substitutions.

## Theoretical Calculations

All calculations have been performed with the Gaussian 03 quantum chemical package[20] using second-order Møller−Plesset perturbation theory (denoted as MP2). For all atoms, the 6-311++G(2d,2p) extended basis set of Pople et al.[21−23] was used. Theoretical study of the $CH_3Cl:H_2O$ complexes has been previously reported by Kryachko et al.[24] using the MP2/6-31+G(d,p) approach. They showed that the global minimum corresponds to a cyclic structure (11.5 kJ/mol) with two hydrogen bonds: the first between the chlorine atom and one of the hydrogens of water and the second between the oxygen atom and one hydrogen of $CH_3Cl$.

In the present study, the optimization of the 1:1 compound without constraint results in two minima: a first one corresponding to the ground state of the complex characterized by two hydrogen bonds (structure 1) and a second structure as a local minimum with only one hydrogen bridge (structure 2). The most significant geometrical parameters of the studied complexes are displayed in Figure 9, and the corresponding

**TABLE 6: Calculated and Experimental Shifts ($cm^{-1}$) of the Vibrational Frequencies of the Two Stable Structures (kJ/mol) of the $CH_3Cl:H_2O$ Complex (Structures 1 and 2)**

| | | structure 1 | structure 2 | exptl |
|---|---|---|---|---|
| $D_e^{BSSE}$ | | 12.7 | 6.6 | |
| $D_0^{BSSE}$ | | 7.3 | 4.2 | |
| C−Cl stretching | $\upsilon_{3\ CH_3Cl}$ | −14.7 | −9.6 | −12.2 |
| C−Cl rocking | $\upsilon_{6\ CH_3Cl}$ | 2.9 | −7.6 | 2.8 |
| | | 15.1 | −4.6 | |
| C−H symmetric bending | $\upsilon_{2\ CH_3Cl}$ | 2.3 | −12.8 | 2.5 |
| C−H antisymmetric bending | $\upsilon_{5\ CH_3Cl}$ | −2.6 | −6.1 | |
| | | 4.1 | −3.0 | 3.7 |
| C−H symmetric stretching | $\upsilon_{1\ CH_3Cl}$ | 2.1 | 12.0 | 4.7 |
| C−H antisymmetric stretching | $\upsilon_{4\ CH_3Cl}$ | 5.7 | 11.8 | 7.5[a] |
| | | 9.6 | 17.4 | |
| O−H bending | $\upsilon_{2\ H_2O}$ | 4.1 | 2.0 | 4.9 |
| O−H symmetric stretching | $\upsilon_{1\ H_2O}$ | −44.1 | −7.8 | −39.6 |
| O−H antisymmetric stretching | $\upsilon_{3\ H_2O}$ | −28.1 | −8.7 | −22.3 |

[a] 7.5 $cm^{-1}$ has to be compared to either 5.7 or 9.6 $cm^{-1}$.

binding energies (corrected for the basis set error, $D_e^{BSSE}$, and for the zero-point energy, $D_0^{BSSE}$) are given in Table 6. The binding energy of structure 1 is found to be 12.7 kJ/mol (very close to that reported by Kryachko et al.[24]), while that of structure 2 is 6.6 kJ/mol. The difference between the stability of the two structures could be due to the fact that, in structure 2, only O and H ($CH_3Cl$) interact, while, in structure 1, there is also an interaction between chlorine and a hydrogen atom of water.

The harmonic frequency shifts calculated with the MP2 method for the two optimized geometries (structures 1 and 2) of the $CH_3Cl:H_2O$ complex and the experimental shifts in neon matrix are listed in Table 6. The calculated vibrational wavenumber shifts for structure 1 are found to reproduce the observed wavenumber shifts more satisfactorily than those for structure 2. The calculated shifts for $H_2O$ in structure 1 are −44.1, +4.1, and −28.1 $cm^{-1}$ for the $\nu_1$, $\nu_2$, and $\nu_3$ modes, respectively, and those for $H_2O$ in structure 2 are −7.8, +2.0, and −8.7 $cm^{-1}$. The measured shifts for the $\nu_1$, $\nu_2$, and $\nu_3$ modes, respectively, are close to those calculated for structure 1: −39.5, +4.9, and −22.3 $cm^{-1}$. The same observation can be made for the wavenumber shifts of the $CH_3Cl:H_2O$ complex from $CH_3Cl$ monomer, calculated for structure 1, which agree essentially with the observed values. These results suggest that the $CH_3Cl:H_2O$ complex isolated in neon matrix corresponds to structure 1. Structure 2 has not been observed experimentally even after annealing the matrix or photoexciting the sample.

Since it can be assumed that the complex has structure 1 and belongs to the $C_1$-symmetry group, the modes of symmetry *E* (in free $CH_3Cl$) are not degenerate anymore and two different frequencies are calculated for the C−Cl rocking, C−H antisymmetric bending, and C−H antisymmetric stretching modes. However, only one frequency was experimentally observed for each mode in the complex. Nevertheless, the absorption bands of $CH_3Cl$ trapped in neon matrix corresponding to these modes are broad and could hide the other absorption bands of the complex.

Finally, we note that the experimental frequency shifts for the C−Cl rocking (+2.8 $cm^{-1}$), C−H symmetric (+2.5 $cm^{-1}$), and C−H antisymmetric (+3.7) bending modes are well reproduced by MP2 calculations for structure 1 (C−Cl rocking, +2.9 $cm^{-1}$; C−H symmetric bending, +2.3 $cm^{-1}$; C−H antisymmetric bending, +4.1 $cm^{-1}$).

The cyclic structure of the 1:1 complex is confirmed in turn by the experimental observations in the C−H and O−H spectral regions. The observed wavenumber shifts imply an intermolecular hydrogen bonding between $CH_3Cl$ and $H_2O$. O−H modes are red shifted which suggests an intermolecular hydrogen bonding between the H atom of $H_2O$ and the Cl atom of $CH_3Cl$. C−H modes are blue shifted which suggests an intermolecular hydrogen bonding between the H atom of $CH_3Cl$ and the O atom of $H_2O$.[24]

**TABLE 7: Calculated and Experimental Shifts ($cm^{-1}$) of the Vibrational Frequencies of the Most Stable Structure (kJ/mol) of the $CH_3Cl:H_2O$ Complex (Structure 1)[a]**

| | structure 1 | experimental |
|---|---|---|
| $CH_3Cl:HOH$ | | |
| $D_0^{BSSE}$ | 7.3 | |
| $\upsilon_2$ (OH bending) | 4.1 | 4.9 |
| $\upsilon_1$ (symmetric OH stretching) | −44.1 | −39.6 |
| $\upsilon_3$ (antisymmetric OH stretching) | −28.1 | −22.3 |
| $CH_3Cl:HOD$ | | |
| $D_0^{BSSE}$ | 7.6 | |
| $\upsilon_2$ (HOD bending) | 15.5 | - |
| $\upsilon_1$ (OD stretching) | −0.8 | - |
| $\upsilon_3$ (OH stretching) | −70.7 | - |
| $CH_3Cl:DOH$ | | |
| $D_0^{BSSE}$ | 8.0 | |
| $\upsilon_2$ (HOD bending) | −7.6 | −4.5 |
| $\upsilon_1$ (OD stretching) | −50.9 | −45.9 |
| $\upsilon_3$ (OH stretching) | −1.4 | −1.8 |
| $CH_3Cl:DOD$ | | |
| $D_0^{BSSE}$ | 8.3 | |
| $\upsilon_2$ (DOD bending) | 1.3 | 1.5 |
| $\upsilon_1$ (symmetric OD stretching) | −29.1 | −26.9 |
| $\upsilon_3$ (antisymmetric OD stretching) | −22.5 | −18.5 |

[a] H/D water isotopic substitution.

Vibrational wavenumbers for the four isotopic complexes $CH_3Cl:H_2O$, $CH_3Cl:HOD$, $CH_3Cl:DOH$, and $CH_3Cl:D_2O$ were calculated for structure 1. The wavenumber shifts are compared with the observed values in Table 7. The calculated shifts agree with the observed values in the case of $CH_3Cl:H_2O$ and $CH_3Cl:D_2O$. However, for the partially deuterated complex, the calculated wavenumbers reproduce the observed wavenumbers only for the $CH_3Cl:DOH$ species, a complex with an intermolecular D bonding. Experimentally, the HOD bending mode in the complex is found to be red shifted by −4.5 $cm^{-1}$ which agrees with $CH_3Cl:DOH$ (calculated shift −7.6 $cm^{-1}$) rather than with $CH_3Cl:HOD$ (calculated shift +15.5 $cm^{-1}$). No infrared bands of $CH_3Cl:HOD$ (complex with an intermolecular H bonding) were observed in our spectra. The absence of any signal from the $CH_3Cl:HOD$ complex in our spectra could be explained by the fact that the dissociation energy of $CH_3Cl:DOH$ is larger than that of $CH_3Cl:HOD$, since the zero-point vibrational energy of the species with D-atom bonding is lower (by 0.4 kJ/mol = 35 $cm^{-1}$) than that of the H-atom one. According to the Boltzmann distribution law, the population ratio at 5 K for this energy difference is found to be $[CH_3Cl:HOD]/[CH_3Cl:DOH] = 0.000\ 05$. This phenomenon was already observed by Nakata et al.[25] who reported the structure of $CH_3F:H_2O$ which is similar to structure 1 for $CH_3Cl:H_2O$. The energy of dimerization of $CH_3F:H_2O$ was found to be 13.6 kJ/ mol. Indeed, in the partially deuterated complexes $CH_3F:DOH$ and $CH_3F:HOD$, Nakata et al.[25] detected only the $CH_3F:DOH$ complex and no bands of $CH_3F:HOD$ were observed. This is also a consequence of the preference for HDO to form HO−D···A (A: electronegative element) deuterium bonds rather than the DO−H···A bonds already discussed in the literature.[26−27]

Finally, we would like to compare the H bonding properties between two complexes: $CH_3Cl:H_2O$ and $H_2O:H_2O$ both

contain a water molecule. The $H_2O$ molecule in $CH_3Cl:H_2O$ is both the proton acceptor (PA, O interacting with H of $CH_3Cl$) and donor (PD, H interacting with Cl). These intermolecular hydrogen bonds could be compared to those of $(H_2O)_2$, where one water molecule is the PA and the other is the PD. The behavior of the $H_2O$ molecule in $CH_3Cl:H_2O$ is expected to range between the PA and PD of $(H_2O)_2$. The OH symmetric mode is red shifted, with respect to $H_2O$ monomer, by $-1.1$ and $-2.1\%$ for $CH_3Cl:H_2O$ and PD $(H_2O)_2$, respectively. The OH stretching mode detected at 3625.9 $cm^{-1}$ for $CH_3Cl:H_2O$ is closer to the proton acceptor (PA, 3660.6 $cm^{-1}$ of $(H_2O)_2$) than to the proton donor (PD, 3590.5 $cm^{-1}$ of $(H_2O)_2$).[14] The OH antisymmetric stretching detected at 3738.8 $cm^{-1}$ for $CH_3Cl:H_2O$ is closer to the proton donor (PD, 3733.7 $cm^{-1}$ of $(H_2O)_2$) than to the proton acceptor (PA, 3750.0 $cm^{-1}$ of $(H_2O)_2$). Finally, the OH bending mode detected at 1600.5 $cm^{-1}$ for $CH_3Cl:H_2O$ is closer to the proton acceptor (PA, 1599.2 $cm^{-1}$ of $(H_2O)_2$) than to the proton donor (PD, 1616.4 $cm^{-1}$ of $(H_2O)_2$). However, by comparing the wavenumber shifts, this "double" intermolecular hydrogen bonding is weaker than that observed in $(H_2O)_2$.

## Conclusion

Formation and structure of the $CH_3Cl:H_2O$ weakly bonded complex has been investigated by the neon matrix isolation technique combined with infrared absorption spectroscopy. Detailed vibrational assignments were made on the observed spectra of water and deuterated water engaged in the $CH_3Cl:H_2O$ complex. With the use of MP2 calculations, the geometrical and vibrational properties of the complex have been estimated. The complex was found to have a cyclic structure, where the chlorine atom is weakly bonded to one of the hydrogen atoms of water, while the oxygen atom is weakly bonded to one of the hydrogen atoms of $CH_3Cl$. The binding energy of $CH_3Cl:H_2O$ is 12.7 kJ/mol. The calculated and observed wavenumbers of the partially deuterated complex established that only the $CH_3Cl:DOH$ species was formed with hydrogen bonding to D. No bands of $CH_3Cl:HOD$ (complex with H bonding) were observed.

## References and Notes

(1) Rosenlof, K. H. *Science* **2001**, *302*, 1691.
(2) Loewenschuss, A.; Givan, A.; Nielsen, C. J. *J. Mol. Struct.* **1997**, *408*, 533.
(3) Coussan, S.; Loutellier, A.; Perchard, J. P.; Racine, S.; Bouteiller, Y. *J. Mol. Struct.* **1998**, *471*, 37.
(4) Chaban, G. M.; Gerber, R. B.; Janda, K. C. *J. Phys. Chem. A* **2001**, *105*, 8323.
(5) Danset, D.; Manceron, L. *J. Phys. Chem. A* **2003**, *107*, 11324.
(6) Dozova, N.; Krim, L.; Alikhani, M. E.; Lacome, N. Manuscript submitted for publication.
(7) Perchard, J. P. *Chem. Phys.* **2001**, *273*, 217.
(8) Michaut, X.; Vasserot, A. M.; Abouaf, M. L. *Vib. Spectrosc.* **2004**, *34*, 83.
(9) Engdahl, A.; Nelander, B. *J. Chem. Phys.* **1989**, *91*, 6604.
(10) Forney, D.; Jacox, M. E.; Thompson, W. E. *J. Mol. Struct.* **1993**, *157*, 479.
(11) Knözinger, E.; Wittenbeck, R. *J. Am. Chem. Soc.* **1983**, *105*, 2154.
(12) Tonkyn, R. G.; Wiedmann, R.; Grant, E. R.; White, M. G. *J. Chem. Phys.* **1991**, *95*, 7033.
(13) Fajardo, M. E.; Tam, S.; Derose, M. E. *J. Mol. Struct.* **2004**, *695*, 111.
(14) Bouteiller, Y.; Perchard, J. P. *Chem. Phys.* **2004**, *305*, 1.
(15) Rothman, L. S.; Rinsland, C. P.; Goldman, A.; Massie, S. T.; Edwards, D. P.; Flaud, J.-M.; Perrin, A.; Camy-Peyret, C.; Dana, V.; Mandin, J.-Y.; Schroeder, J.; McCann, A.; Gamache, R. R.; Wattson, P. B.; Yoshino, K.; Chance, K. V.; Jucks, K. W.; Brown, L. R.; Nemtchinov, V.; Varanasi, P. *J. Quant. Spectrosc. Radiat. Transfer* **1998**, *60*, 665.
(16) Bykov, A. D.; Makarov, V. S.; Moskalenko, N. I.; Naumenko, O. V.; Ulenikov, O. N.; Zotov, O. V. *J. Mol. Spectrosc.* **1987**, *123*, 126.
(17) Toth, R. A. *J. Mol. Spectrosc.* **1999**, *195*, 98.
(18) He, S.; Ulenikov, O. N.; Onopenko, G. A.; Bekhtereva, E. S.; Wang, X.; Hu, S.; Lin, H.; Zhu, Q. *J. Mol. Spectrosc.* **2000**, *200*, 34.
(19) Toth, R. A. *J. Mol. Spectrosc.* **1999**, *195*, 73.
(20) Frisch, M. J.; Trucks, G. W.; Schlegel, H. B.; Scuseria, G. E.; Robb, M. A.; Cheeseman, J. R.; Montgomery, J. A., Jr.; Vreven, T.; Kudin, K. N.; Burant, J. C.; Millam, J. M.; Iyengar, S. S.; Tomasi, J.; Barone, V.; Mennucci, B.; Cossi, M.; Scalmani, G.; Rega, N.; Petersson, G. A.; Nakatsuji, H.; Hada, M.; Ehara, M.; Toyota, K.; Fukuda, R.; Hasegawa, J.; Ishida, M.; Nakajima, T.; Honda, Y.; Kitao, O.; Nakai, H.; Klene, M.; Li, X.; Knox, J. E.; Hratchian, H. P.; Cross, J. B.; Bakken, V.; Adamo, C.; Jaramillo, J.; Gomperts, R.; Stratmann, R. E.; Yazyev, O.; Austin, A. J.; Cammi, R.; Pomelli, C.; Ochterski, J. W.; Ayala, P. Y.; Morokuma, K.; Voth, G. A.; Salvador, P.; Dannenberg, J. J.; Zakrzewski, V. G.; Dapprich, S.; Daniels, A. D.; Strain, M. C.; Farkas, O.; Malick, D. K.; Rabuck, A. D.; Raghavachari, K.; Foresman, J. B.; Ortiz, J. V.; Cui, Q.; Baboul, A. G.; Clifford, S.; Cioslowski, J.; Stefanov, B. B.; Liu, G.; Liashenko, A.; Piskorz, P.; Komaromi, I.; Martin, R. L.; Fox, D. J.; Keith, T.; Al-Laham, M. A.; Peng, C. Y.; Nanayakkara, A.; Challacombe, M.; Gill, P. M. W.; Johnson, B.; Chen, W.; Wong, M. W.; Gonzalez, C.; Pople, J. A. *Gaussian 03*, revision B.02; Gaussian, Inc.: Pittsburgh, PA, 2003.
(21) Krishnan, R. J.; Binkley, S.; Seeger, R.; Pople, J. A. *J. Chem. Phys.* **1980**, *72*, 650.
(22) Clark, T.; Chandrasekhar, J.; Spitznagel, G. W.; Schleyer, P. V. R. *J. Comput. Chem.* **1983**, *4*, 294.
(23) Frisch, M. J.; Pople, J. A.; Binkley, J. S. *J. Chem. Phys.* **1984**, *80*, 3265.
(24) Kryachko, E. S.; Huyskens, Z. T. *J. Phys. Chem. A* **2001**, *105*, 7118.
(25) Futami, Y.; Kudoh, S.; Takayanagi, M.; Nakata, M. *Chem. Phys. Lett.* **2002**, *357*, 209.
(26) Ayers, G. P.; Pullin, A. D. E. *Spectrochim. Acta, Part A* **1976**, *32*, 1695.
(27) Diken, E. G.; Shin, J. W.; Price, E. A.; Johnson, M. A. *Chem. Phys. Lett.* **2004**, *387*, 17.